Journal of Anatomy

J. Anat. (2010) **217**, pp715–727 doi: 10.1111/j.1469-7580.2010.01307.x

Vertebral microanatomy in squamates: structure, growth and ecological correlates

Alexandra Houssaye,[1] Arnaud Mazurier,[2] Anthony Herrel,[3] Virginie Volpato,[4] Paul Tafforeau,[5] Renaud Boistel[3,5] and Vivian de Buffrénil[1]

[1]*UMR 7207 du CNRS, Département Histoire de la Terre, Muséum National d'Histoire Naturelle, Paris, France*
[2]*Etudes Recherches Matériaux, Poitiers Cedex, France*
[3]*UMR 7179 du CNRS, Département Ecologie et Gestion de la Biodiversité, Muséum National d'Histoire Naturelle, Paris, France*
[4]*Abteilung Paläoanthropologie und Messelforschung, Senckenberg Forschungsinstitut und Naturmuseum, Frankfurt am Main, Germany*
[5]*European Synchrotron Radiation Facility, BP220, Grenoble, France*

Abstract

The histological study of vertebrae in extant squamates shows that the internal vertebral structure in this group differs from that of other tetrapods. Squamate vertebrae are lightly built and basically composed of two roughly concentric osseous tubes – one surrounding the neural canal and the other constituting the peripheral cortex of the vertebra – connected by few thin trabeculae. This structure, which characteristically evokes that of a tubular bone, results from a peculiar remodelling process characterised by an imbalance between local bone resorption and redeposition; in both periosteal and endosteo-endochondral territories, bone is extensively resorbed but not reconstructed in the same proportion by secondary deposits. This process is particularly intense in the deep region of the centrum, where originally compact cortices are made cancellous, and where the endochondral spongiosa is very loose. This remodelling process starts at an early stage of development and remains active throughout subsequent growth. The growth of squamate centra is also strongly asymmetrical, with the posterior (condylar) part growing much faster than the anterior (cotylar) part. Preliminary analyses testing for associations between vertebral structure and habitat use suggest that vertebrae of fossorial taxa are denser than those of terrestrial taxa, those in aquatic taxa being of intermediate density. However, phylogenetically informed analyses do not corroborate these findings, thus suggesting a strong phylogenetic signal in the data. As our analyses demonstrate that vertebrae in snakes are generally denser than those of lizards *sensu stricto*, this may drive the presence of a phylogenetic signal in the data. More comprehensive sampling of fossorial and aquatic lizards is clearly needed to more rigorously evaluate these patterns.

Key words ecology; growth; histology; microanatomy; squamates; vertebrae.

Introduction

Vertebral inner structure and architecture have received little attention from a comparative perspective, especially in non-mammalian tetrapods. In tetrapods in general, the vertebral mass accounts for an important part (20–60%) of the total skeletal mass, thus contributing significantly to body inertia (de Buffrénil et al. 1986). Moreover, the axial skeleton and musculature play a major role in locomotion, particularly in limbless taxa and in animals with a sprawling gait such as lizards (Gasc, 1977; Ritter, 1996). The vertebrae of extant squamates were studied morphologically by Hoffstetter & Gasc (1969), and functionally by Gasc (1976, 1977) and Moon (1999). However, their microanatomical and histological features were not described in detail, with the exception of some brief mentions by de Buffrénil & Rage (1993), de Buffrénil et al. (2008) and Houssaye et al. (2008). More generally, histological studies of bone tissue in squamates are relatively rare compared with those dealing with other amniotes.

The aim of the present study was first to document the inner structure of squamate vertebral centra at a broad comparative scale. Subsequently, our goal was to interpret the osteogenic processes involved in squamate vertebral growth using histological and microanatomical approaches. We highlight those features that are characteristic of squamate vertebrae and distinguish them from other amniotes.

Correspondence
Alexandra Houssaye, Département Histoire de la Terre, Muséum National d'Histoire Naturelle, 57 rue Cuvier, CP-38, 75000 Paris, France. T: 0033140793458; F: 0033140793580; E: houssaye@mnhn.fr

Accepted for publication *13 September 2010*
Article published online *12 October 2010*

Additionally, we explore whether vertebral compactness and architecture are related to habitat use in squamates, as would be predicted based on the mechanics of locomotion in different media. Specifically, we predict the vertebrae in fossorial taxa to be relatively compact, as the axial skeleton is used to transmit often considerable forces (O'Reilly et al. 1997) from the animal to the external environment and needs to dissipate the reaction forces generated during burrowing. However, terrestrial and climbing taxa would benefit from relatively light vertebrae as this would allow them to minimise their overall mass, which would enable them to maximise locomotor velocity and would reduce the cost of transport. Aquatic taxa are faced with fewer constraints on skeletal mass due to the buoyant forces of water and consequently we predict these animals to have vertebrae of intermediate compactness. Finally, we test whether lizards and snakes differ in the structure and growth of their vertebrae. Preliminary analyses (personal observations) indeed suggested some differences in vertebral internal architecture between these two groups.

Materials and methods

Materials

The biological material consisted of a set of dorsal vertebrae from various extant squamate taxa from the collections of comparative anatomy and herpetology of the Muséum National d'Histoire Naturelle (Paris, France) and the Museum Alexander Koenig (Bonn, Germany) (cf. Table 1). Our sample included 45 species (39 genera) representative of the main groups of squamates. Each species is represented by one or several specimens, and each specimen is generally represented by two or three contiguous dorsal vertebrae. In addition to collection specimens, one very young specimen of *Varanus exanthematicus* [snout–vent length = 155 mm; technical details in Castanet (1982)] was injected intra-peritoneally with fluorochromes (fluorescein and xylenol orange) to investigate skeletal growth *in vivo*. This specimen was also used to assess the juvenile state of vertebral microanatomy. Comparative material consisted of dorsal vertebrae from diverse amniotes with distinct functional adaptations (Table 2): *Crocodylus niloticus* (Nile crocodile), *Aptenodytes patagonicus* (king penguin), *Oryctolagus cuniculus* (European rabbit), *Vulpes vulpes* (red fox), *Meles meles* (European badger), *Enhydra lutris* (sea otter), *Otaria byronia* (South American sea lion), *Cephalophus monticola* (blue duiker), *Capreolus capreolus* (European roe deer) and *Macaca* sp. (macaque). Moreover, additional published references of vertebral sections of *Homo sapiens* and *Rattus norvegicus* (brown rat) were used for comparative purposes (Heggeness & Doherty, 1997; Hengsberger et al. 2005).

Methods

Histology

Longitudinal and transverse thin sections (80–100 μm thick) of the vertebrae were made using standard techniques (see de Buffrénil et al. 2008; Figs 1 and 3) at the University Pierre et Marie Curie (Paris, France). Vertebrae were sectioned in the mid-sagittal and the so-called neutral transverse (de Buffrénil et al. 2008) planes (Fig. 1). The sections were examined microscopically (Zeiss Axioskop and Nikon Eclipse 800 microscopes) at low and medium magnification (25–100×) in natural and polarised transmitted light.

Microtomography

For some specimens (cf. Table 1), data were acquired by means of conventional and synchrotron X-ray microtomography, allowing a non-destructive imaging of the 3D outer and inner structure of the samples. Two different set-ups were used (Table 1): (i) laboratory microtomography at the University of Poitiers (France), using an X8050-16 Viscom model [resolution between 16.7 and 32.3 μm; reconstructions performed using Feldkamp algorithm with DigiCT software, version 1.15 (Digisens SA, France)] at the Etudes-Recherches-Matériaux laboratory (Poitiers, France; http://www.erm-poitiers.fr); and (ii) third-generation synchrotron microtomography (Mazurier et al. 2006; Tafforeau et al. 2006) at the European Synchrotron Radiation Facility (ESRF) (Grenoble, France), on beamline ID 19 (resolution 7.46 μm; reconstruction performed using filtered back-projection algorithm with the ESRF PyHST software). Image segmentation and visualisation were performed using Amira software, version 4.1.1 (Mercury Computer Systems, Chelmsford, MA, USA).

Quantitative analysis

Sections were drawn to scale (with a camera lucida Zeiss Stemi SV6 or via photographs) and measurements were made either directly on the bones [centrum length (CL)] or on the sections [index describing the position of the neutral point (NPPi) and centrum proportion index (CPi)]. Additional variables were obtained for analysis using the software ImageJ (Abramoff et al. 2004). The total data set consisted of the following.

1 The length of the centrum between the condylar and cotylar rims (CL), which is used as an indicator of specimen size.

This index was also used as an estimate of size for the transverse sections for all specimens for which longitudinal and transverse sections come from either the same vertebra or from consecutive vertebrae in the same specimen, assuming that CL should be relatively similar between consecutive vertebrae.

2 A NPPi, calculated as the maximal distance from the neutral transverse plane to the condylar rim $\times$ 100/CL. This index provides information regarding the degree of asymmetry of the growth in length of the centrum.

3 The CPi, calculated as centrum height divided by CL. This index describes the differential growth in length and diameter.

4 The global compactness in transverse section (Cts), calculated as the total sectional area minus the area occupied by cavities and the neural canal multiplied by 100 and divided by the total area minus the area occupied by the neural canal.

5 The global compactness of the centrum in longitudinal section (Cls), calculated as the total area of the centrum minus the area occupied by cavities multiplied by 100 and divided by the total area of the centrum.

6 The total number of cavities in longitudinal section (TNCL).

7 The total number of cavities in transverse section (TNCT), with both TNCL and TNCT providing information about the vertebral inner organisation.

Table 1 List of the material analysed with corresponding indices.

Family	Taxon	Adult total length (cm)	Collection reference	Cls	PBCL	TNCL	CL (mm)	Cts	PBCT	TNCT	Cpi	NPPi
Iguanidae	*Amblyrhynchus cristatus*[1]	60–130	ZFMK 10834	55.8	10.0	128	13.2	44.6	33.3	27	29.5	58.5
			ZFMK 10850	54.2	8.7	108	15.1	49.9	34.5	24	25.5	61.7
			ZFMK 10865	68.2	10.6	158	11.5	61.7	31.3	83	26.8	80.5
	Dipsosaurus dorsalis[1]	~ 40	MNHN AC 1944 73	77.1	26.6	32	0.9	69.2	59.8	5	–	–
	Iguana delicatissima[1]	40–80	Unnumbered[2]	57.1	–	86	13.6	66.3	–	42	–	–
	Iguana iguana[1]	150–200	MNHN AC 1939 523[2]	72.5	–	–	13.6	83.5	–	–	–	–
			Unnumbered[2]	58.9	–	102	13.6	55.0	–	44	–	–
Polychrotidae	*Anolis sagrei*	< 20	MNHN SQ-Vert 1	–	–	–	–	52.3	–	8	–	–
Agamidae	*Agama atra*[1]	~ 20	MNHN AC 1887 881	50.5	19.2	17	4.6	65.9	–	8	23	67.8
	Agama impalearis	20–25	MNHN AC 1942 101	–	–	–	–	69.2	55.0	5	–	–
	Physignathus cocincinus[1]	80–100	MNHN SQ-Vert 2	55.7	12.8	9	1.9	45.7	–	9	31.4	85.1
Chamaeleonidae	*Brookesia minima*[1]	2.8–3.3	MNHN 1988 0876[3]	70.7	–	3	0.6	82.9	–	3	–	–
	Calumma nasutum[1]	< 11	MNHN 6643F[3]	47.5	–	27	1.9	72.4	–	6	–	–
	Furcifer campani[1]	< 13	MNHN 1970 1053[3]	52.5	–	2	0.8	78.2	–	5	–	–
Gekkonidae	*Coleonyx elegans*	~ 20	MNHN AC 1996 6378	57.6	–	41	2.7	–	–	–	–	–
	Eublepharis macularius	20–25	MNHN SQ-Vert 3	–	–	–	–	57.6	53.8	23	–	–
				–	–	–	–	60.6	–	21	–	–
	Strophurus spinigerus	< 10	MNHN AC 1997 3257	–	–	–	–	71.2	–	11	–	–
Lacertidae	*Gallotia simonyi*[1]	~ 60	MNHN SQ-Vert 4	69.8	12.1	64	8.9	58.7	40.9	28	29.3	72.9
				68.5	11.6	51	9.1	45.3	28.5	18	27.9	65.4
	Timon lepidus[1]	60–80	MNHN AC 1973 106	63.2	15.7	40	4.8	83.6	64.8	30	29.1	70.1
Amphisbaenidae	*Amphisbaena alba*[1]	~ 75	MNHN AC 1986 0204	73.1	–	43	4.9	86.6	54.9	13	–	–
				–	–	–	–	81.5	–	27	–	–
Teiidae	*Ameiva ameiva*	40–50	MNHN AC 1887 875	67.9	24.6	17	2.5	–	–	–	32	78.2
				79.7	15.4	16	2.6	–	–	–	11.5	72.0
	Tupinambis teguixin[1]	80–100	MNHN AC 1920 108	48.0	10.9	57	7.3	49.3	28.3	27	26.9	83.8
			MNHN AC 1920 108[2]	51.6	–	44	6.8	59.4	–	40	–	–
			MNHN AC 1883 1846	52.6	13.5	60	7.7	51.5	36.0	22	25.9	63.2
			MNHN AC 1883 1846[2]	57.3	–	68	11.0	55.5	–	44	–	–
			MNHN AC 1967 24	43.5	12.0	45	11.6	40.3	29.3	8	36.6	83.7
				–	–	–	–	41.3	27.2	8	–	–
Scincidae	*Scincus scincus*[1]	~ 20	MNHN SQ-Vert 5	50.8	21.3	11	3.0	62.3	44.6	7	37.2	–
	Tribolonotus gracilis[1]	15–20	MNHN 2003-0882[3]	60.7	–	13	0.5	59.5	–	19	–	–
Anguidae	*Anguis fragilis*[1]	40–50	MNHN AC 1996 0199	47.5	10.0	17	3.8	65.2	–	26	36.2	69.3
Xenosauridae	*Shinisaurus crocodilurus*	30–40	MNHN AC 1996 2716	60.5	21.2	21	3.1	–	–	–	26.1	85.4
Varanidae	*Varanus bengalensis*[1]	100–150	MNHN AC 1883-1828	55.1	23.6	80	13.1	–	–	–	36.1	78.4
				59.7	21.1	81	11.4	–	–	–	28.7	81.5
				59.8	26.3	84	11.2	58.1	38.3	46	26.6	82.9
	Varanus doreanus[1]	130–160	ZFMK 9818[2]	60.7	–	38	12.1	53.7	–	12	–	–

Table 1 Continued.

Family	Taxon	Adult total length (cm)	Collection reference	Cls	PBCL	TNCT	CL (mm)	Cts	PBCT	TNCT	Cpi	NPPi
	Varanus exanthematicus	80–100	MNHN AC 1910-71	63.9	26.3	118	12.2	–	–	–	27.7	62.1
			MNHN SQ-Vert 6	60.5	14.8	32	4.4	–	–	–	16.3	83.7
	Varanus griseus[1]	80–140	MNHN AC 1888-196	38.5	15.4	32	9.5	42.6	32.0	13	27.8	82.4
	Varanus niloticus	150–200	MNHN AC 1977-03	60.3	26.0	40	11.9	–	–	–	26.4	77.3
Boidae	*Broghammerus reticulatus*[1]	370–500	MNHN AC 1931 70	72.6	31.8	154	16.5	–	–	–	61.8	71.5
			MNHN AC 1931 69	73.2	30.7	59	11.6	–	–	–	59.8	67.6
			MNHN AC 2002 18	72.9	35.3	46	5.9	69.5	52.7	7	70.9	67.2
				–	–	–	–	70.4	56.1	9	–	–
			MNHN SQ-Vert 11	72.0	30.2	56	12.3	–	–	–	60	–
			MNHN SQ-Vert 12	–	–	–	–	84.9	71.0	5	–	–
			MNHN SQ-Vert 13	–	–	–	–	70.5	46.0	34	–	–
	Eryx jaculus[1]	45–60	MNHN AC 2005 58	71.9	22.6	34	3.9	78.8	46.9	31	54.6	65.4
			MNHN SQ-Vert 7	79.4	36.2	20	4.2	–	–	–	41.4	63.6
			MNHN SQ-Vert 8	76.2	31.7	27	4.4	–	–	–	–	–
	Eunectes murinus[1]	300–700	MNHN AC 1893 197	69.1	27.1	77	9.0	73.8	52.8	20	64.6	72.2
			MNHN AC 1940 353	69.1	33.7	64	14.3	–	–	–	63	79.9
			MNHN SQ-Vert 9	58.0	21.7	131	15.8	78.4	51.2	16	53.8	77.8
	Morelia viridis[1]	150–200	MNHN SQ-Vert 10	63.7	28.4	13	2.4	79.0	51.0	12	47.2	76.4
				–	–	–	–	68.5	54.7	4	–	–
Aniliidae	*Anilius scytale*[1]	~ 70	MNHN 1996 2701	82.0	38.5	20	3.6	–	–	–	28.3	60.8
			MNHN 1996 2701[2]	66.8	–	26	3.7	77.3	–	12	–	–
Cylindrophiidae	*Cylindrophis ruffus*[1]	40–80	MNHN 1998 0201	80.6	36.2	25	2.9	96.1	86.9	6	41.8	73.8
Xenopeltidae	*Xenopeltis unicolor*[1]	100	MNHN 1990 5174	72.6	41.6	13	2.1	85.4	92.4	5	34.7	80.2
Acrochordidae	*Acrochordus javanicus*[1]	150–250	MNHN SQ-Vert 14	66.8	38.6	35	8.4	77.5	57.1	12	41.3	61.1
Atractaspididae	*Atractaspis microlepidota*	45–75	MNHN 1999 8559	–	–	–	–	70.2	64.5	4	–	–
Colubridae s. l	*Enhydris bocourti*[1]	~ 100	MNHN 1999 8361	78.9	46.0	30	3.8	87.7	–	9	57.3	76.6
	Enhydris plumbea[1]	~ 50	ZFMK 44891	70.0	43.4	23	2.9	79.9	67.5	5	38.1	80.5
				–	–	–	–	64.8	–	6	–	–
	Natrix natrix	60–100	MNHN AC 1874 535	73.0	25.9	39	5.3	–	–	–	29.4	63.0
	Pantherophis guttatus[1]	120–200	MNHN SQ-Vert 15	42.5	10.8	6	1.1	67.5	40.7	5	39.8	–
				53.5	–	7	1.1	–	–	–	–	–
				61.2	19.5	8	1.2	–	–	–	31	70.6
	Pareas carinatus	60–70	MNHN 2000 4272	–	–	–	–	76.6	60.4	4	–	–
Elapidae	*Dendroaspis jamesoni*[1]	180–270	MNHN SQ-Vert 16	76.6	28.7	24	6.0	72.4	61.9	6	20.7	81.3
				67.7	26.2	33	5.8	–	–	–	26.8	80.4
	Hydrophis sp.[1]		MNHN AC 1887 897	–	–	–	–	84.0	69.9	3	–	–
			MNHN SQ-Vert 18	88.8	39.7	32	4.4	84.2	73.1	5	30.4	68.2
	Laticauda laticaudata[1]	90–110	ZFMK 36425	72.5	29.2	20	3.1	87.2	77.5	3	26.4	75.2

Table 1 Continued.

Family	Taxon	Adult total length (cm)	Collection reference	Cls	PBCL	TNCT	CL (mm)	Cts	PBCT	TNCT	Cpi	NPPi
				66.2	25.3	16	2.9	74.5	62.4	3	32.3	68.9
	Ophiophagus hannah[1]	300–450	MNHN SQ-Vert 17	65.8	30.0	66	11.9	64.4	55.7	5	39.3	79.1
			MNHN AC 2002-42[2]	75.2	–	85	12.5	72.1	–	26	–	–
	Pelamis platura	70–90	ZFMK 36436	54.9	16.3	27	2.3	–	–	–	30.8	81.7
Viperidae	*Agkistrodon piscivorus*[1]	~ 80	MNHN 1990 3854	68.0	–	63	7.5	64.3	–	11	–	–
	Bitis arietans[1]	100–150	MNHN AC 1885 246	84.8	55.2	106	8.5	77.4	–	19	57.1	81.4
			MNHN AC 1977 13	84.3	48.8	66	9.2	–	–	–	56.5	76.5
			MNHN SQ-Vert 19	73.7	39.0	50	9.1	–	–	–	68.8	–
	Bothrops lanceolatus[1]	100–200	MNHN AC 1887 934	71.0	40.2	50	7.1	65.8	49.4	12	52.8	77.4
				–	–	–	–	67.4	50.9	12	–	–

Cls, global compactness of the centrum in longitudinal section; PBCL, relative area of primary periosteal bone in longitudinal section; TNCL, total number of cavities in longitudinal section; CL, centrum length; Cts, global compactness in transverse section; PBCT, relative area of primary periosteal bone in transverse section; TNCT, total number of cavities in transverse section; CPi, centrum proportion index; NPPi, index describing the position of the neutral point.
[1]Species included in the phylogenetically informed regression analyses.
[2,3]Specimens for which conventional or synchrotron X-ray microtomography was used.

8 The relative area of primary periosteal (= cortical) bone in transverse section (PBCT), calculated as the area occupied by primary periosteal bone multiplied by 100 and divided by the total vertebral area minus the area occupied by the neural canal.

9 The relative area of primary periosteal bone in longitudinal section (PBCL), calculated as the area occupied by primary periosteal bone multiplied by 100 and divided by the total area of the centrum. Both PBCT and PBCL provide insights into the process of bone remodelling. These last two indices could not be measured on virtual sections and were not determined for histological sections where the contrast between the two types of osseous tissues could not be clearly distinguished.

Statistical analyses

All data were $\log_{10}$ transformed prior to analyses to meet assumptions of normality and homoscedascity required for parametric analyses. To describe relationships between vertebral microstructure, size and compactness, we first used traditional regression analyses performed on the raw data set (Figs 6–8). However, as species are not independent data points but related through their evolutionary history, we next performed phylogenetically informed regression analyses on the independent contrasts for a subset of the data. All data points used in the phylogenetic analysis consisted of the species means. Only those taxa for which all variables could be determined were included in the phylogenetic analysis (Table 1; Fig. 2).

Independent contrasts were calculated using the PDAP package (Garland et al. 1999) and all regressions were forced through the origin. The phylogenetic framework for these analyses was based on Lee et al. (2007) and Lee (2009) for the interfamilial relationships and on Wiens & Hollingsworth (2000), Ast (2001), Castoe & Parkinson (2006) and Kelly et al. (2009) for within-families relationships. All branch lengths were set to 1 as branch lengths were not available for all taxa included in our analysis. To check whether branch lengths of unit length were indeed appropriate for our analyses, we used the diagnostics options in the PDTREE program to test for correlations between the absolute values of the standardised contrasts and their SDs (Garland et al. 1992). As correlations were not significant, these branch lengths could be used (Garland et al. 1992). Moreover, it has been shown that the actual length of the branches does not usually have substantial effects on the results of phylogenetic analyses (Martins & Garland, 1991; Diaz-Uriarte & Garland, 1998).

To test whether vertebral microstructure differed in taxa adapted to different habitats, we classified each species as belonging to one of the following habitat groups: terrestrial, aquatic, fossorial, climber (i.e. both arboreal and saxicolous) and generalist. Phylogenetic analyses of (co)variance involving simulation analyses were performed using the PDSIMUL and PDANOVA programs (Garland et al. 1993). In the PDSIMUL program, we used Brownian motion as our model for evolutionary change and ran 1000 unbounded simulations to create an empirical null distribution against which the *F*-value from the original data could be compared. In the PDANOVA program, habitat use was entered as the dependent variable, vertebral microanatomical characteristics (Cts, Cls, TNCT, TNCL) were used as independent variables, and CL was used as a covariate where appropriate. We considered differences among categories to be significant if the original *F*-value derived from a non-phylogenetic analysis was higher

Table 2 Comparative material of non-squamate amniotes.

Family	Taxon	Collection reference	New sections	μCT resolution (μm)
Crocodylidae	*Crocodylus niloticus*	MNHN AC 1964-403		73.1
		Unnumbered UPMC	LS	
Spheniscidae	*Aptenodytes patagonicus*	Unnumbered UPMC	LS TS	
Leporidae	*Oryctolagus cuniculus*	Unnumbered UPMC	LS TS	
Canidae	*Vulpes vulpes*	Unnumbered UPMC	LS	
Mustelidae	*Meles meles*	MNHN AC (no ref.)	LS	
	Enhydra lutris	MNHN AC (no ref.)		50.1
Otariidae	*Otaria byronia*	MNHN AC 1884-862		50.7
Bovidae	*Cephalophus monticola*	MNHN AC (no ref.)	LS TS	
Cervidae	*Capreolus capreolus*	MNHN AC (no ref.)		73.1
Cercopithecidae	Macaca *sp.*	Unnumbered UPMC	LS TS	

AC, collections of comparative anatomy of the Muséum National d'Histoire Naturelle (MNHN) (Paris, France); LS, longitudinal section; TS, transverse section. Resolution is provided for microtomographic (μCT) data.

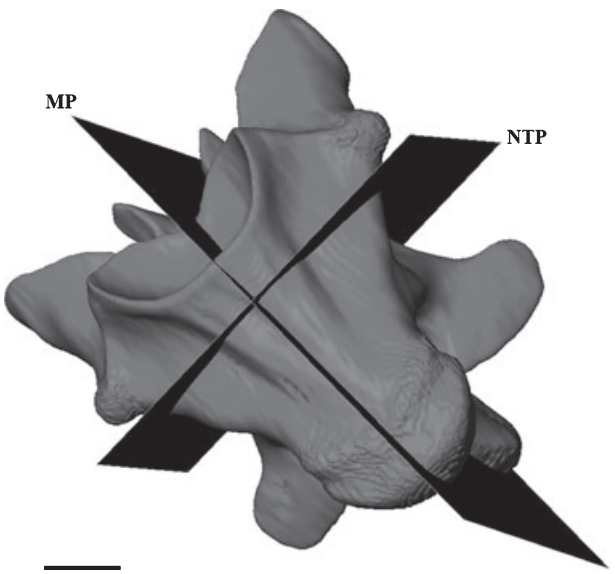

Fig. 1 *Amblyrhynchus cristatus*. 3D imaging of a vertebra in ventral view. The sectional planes are represented in black. MP, midsagittal plane; NTP, neutral transverse plane. Scale bar = 5 mm.

than the F95 value derived from the empirical distribution. All traditional (i.e. non-phylogenetic) analyses were performed with SPSS v.15.

Finally, we tested for differences in vertebral structure between lizards and snakes given (i) the many morphological and ecological differences between these groups, and (ii) prior observations that these groups might differ in vertebral structure. As this comparison is essentially a comparison between two groups, only non-phylogenetic statistics were performed using SPSS v.15.

Results

The vertebrae of all squamates examined consisted of the same type of osseous tissues and had a similar microstructural organisation (see below), regardless of their position along the vertebral column. In the following paragraphs we first provide a qualitative description of the vertebral microanatomy and next a quantitative analysis of the vertebral microstructure.

Qualitative analysis

Longitudinal sections

Three distinct tissue formations can be observed in longitudinal sections (Fig. 3A): (i) compact osseous tissue of periosteal (= cortical) origin located along the ventral edge of the centrum and in a smaller amount also along the floor of the neural canal (particularly just above the cotyle), (ii) layers of hypertrophied calcified cartilage (between 90 and 550 μm thick) bordering the articular surfaces (cotyle and condyle), and (iii) cancellous bone formation of endosteochondral origin occupying the remainder of the sectional area.

In polarised light, periosteal deposits display similar histological features in all specimens: a mass birefringence, and spindle-like osteocyte lacunae, all oriented parallel to the direction of bone deposition (Fig. 4A). These features are characteristic of parallel-fibered (or pseudolamellar) osseous tissue. Cell lacunae are extensive and connected by numerous canaliculi typically oriented parallel to each other. Clear growth marks, corresponding to lines of arrested growth, are observable in the bone matrix. In small animals (e.g. *Agama*, *Eryx*, *Timon*), primary periosteal deposits are avascular, whereas in large animals (*Eunectes*, *Broghammerus*, *Tupinambis*, *Varanus*), they house simple vascular canals (10–60 μm in diameter) oriented radially (Fig. 4B), and sparse primary osteons. Obliquely oriented Sharpey's fibres are particularly abundant at the cranial and caudal extremities of the cortex.

Most of the centrum, in both periosteal and endosteal territories, is occupied by a notably loose spongiosa with

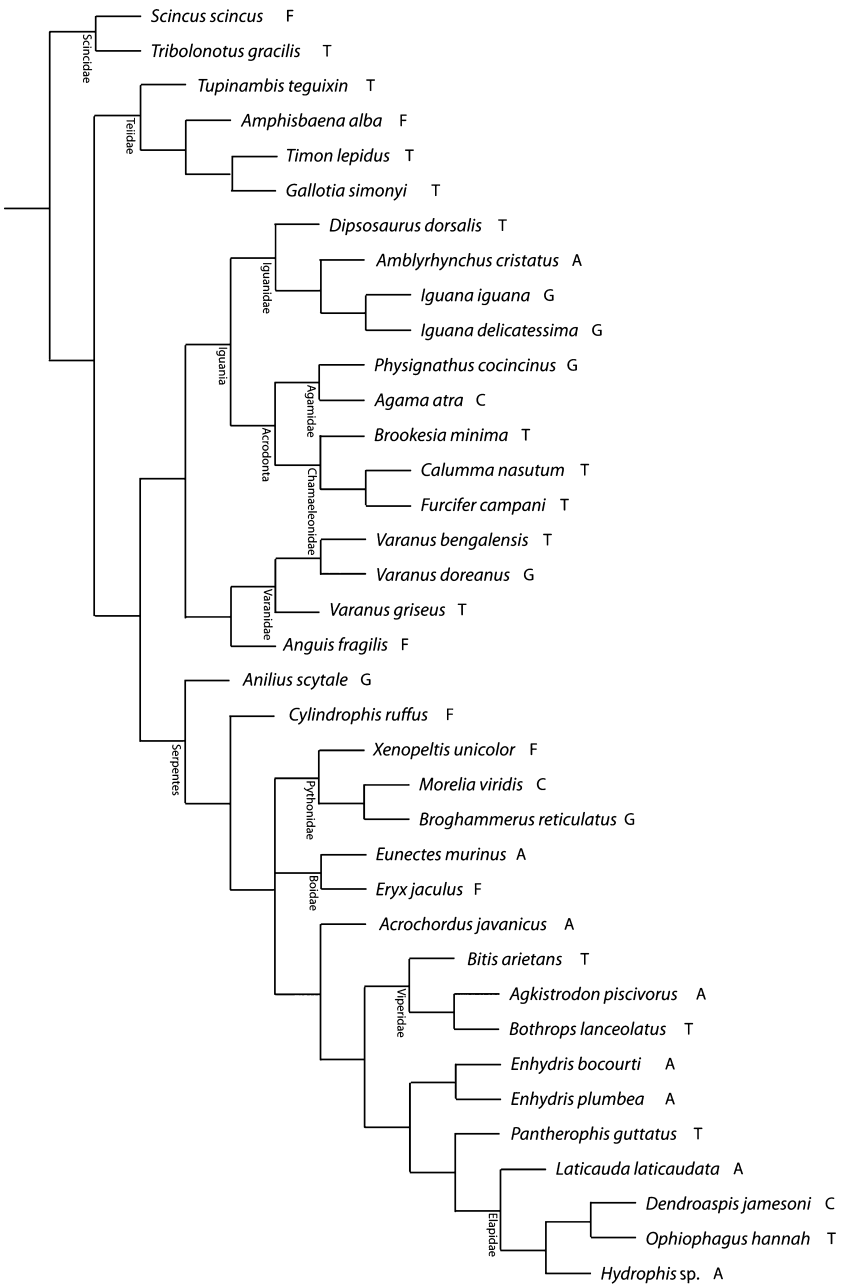

Fig. 2 Phylogenetic tree based on previously published data (Wiens & Hollingsworth, 2000; Ast, 2001; Castoe & Parkinson, 2006; Lee et al. 2007; Kelly et al. 2009; Lee, 2009) and used for the phylogenetically informed analyses (see Materials and methods for details) with indications about the mode of life: A, aquatic; C, climber; F, fossorial; G, generalist; T, terrestrial.

wide randomly shaped inter-trabecular spaces, particularly large towards the core of the centrum (Fig. 3A). In the periosteal territory, the transition from a compact to a cancellous organisation is clearly due to resorption as demonstrated by the numerous Howship's lacunae (Fig. 4B), which are the result of an intense osteoclastic activity. In the ventral part of the spongiosa, the trabeculae consist of a core of parallel-fibered bone plated by endosteal deposits of lamellar tissue (as shown by its alternated extinction in polarised light). Deeper, the trabeculae are exclusively formed by an intensely remodelled lamellar endosteal tissue with no remains of parallel-fibered bone. These trabeculae are therefore completely secondary in origin. Thus, a gradient of trabecular remodelling exists, which changes from the periphery to the depth of the centrum in parallel with a gradient of porosity. In the endosteo-enchondral territory close to the cotylar and condylar surfaces, the core of the trabeculae consists of calcified cartilage (Fig. 4C) covered by irregular platings of endosteal avascular lamellar tissue. Osteocyte lacunae are rich in canaliculi, fusiform and elongated in the direction of bone deposition. Numerous cementing lines (due to resorption) and Howship's lacunae suggest an intense remodelling of the trabeculae (Fig. 4D). As a consequence, calcified cartilage remains are absent even at a short distance from the cotylar and condylar surfaces.

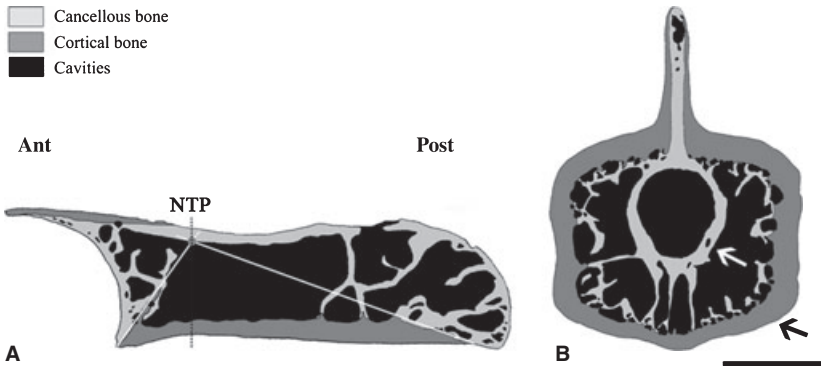

Fig. 3 (A) *Varanus griseus*. MNHN AC 1888-196. Schematic drawing of the longitudinal section of the centrum. The point corresponds to the estimated 'neutral point' and the lines delimit the triangles of growth. NTP, neutral transverse plane. Scale bar = 1.8 mm. (B) *Varanus bengalensis*. MNHN AC 1883-1828. Schematic drawing of the transverse section. The two arrows point to the two osseous rings. Scale bar = 3.1 mm.

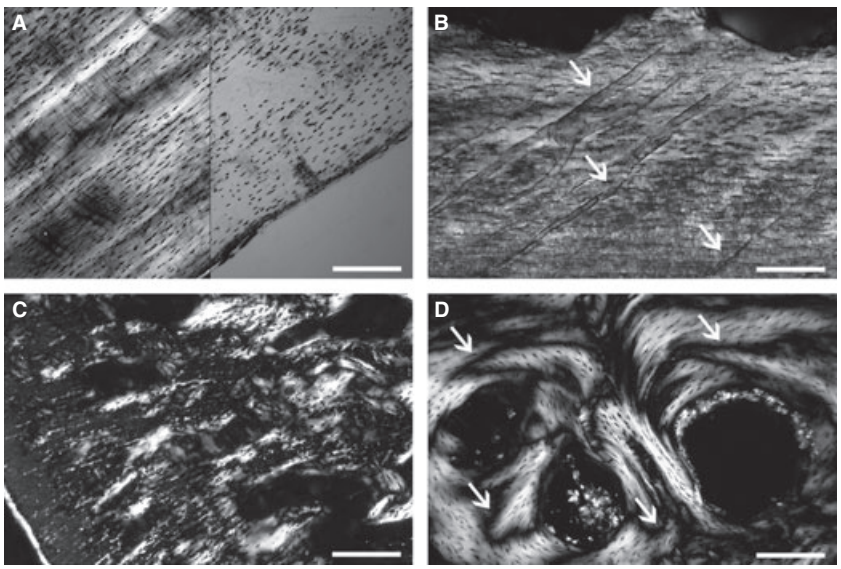

Fig. 4 Longitudinal sections of (A, C, D) *Varanus exanthematicus* and (B) *Varanus griseus*. (A) Primary (pseudolamellar) periosteal bone in polarised (left) and natural (right) light. Note the mass birefringence and the parallel spindle-like osteocytes. Scale bar = 0.3 mm. (B) Primary periosteal bone in polarised light. The arrows point to vascular canals. Howship's lacunae are visible on the top of the primary formation. Scale bar = 0.2 mm. (C) Calcified cartilage in the core of trabeculae of endosteo-enchondral origin in polarised light. Scale bar = 0.3 mm. (D) Highly remodelled lamellar bone in polarised light. The arrows point to cementing lines of resorption. Scale bar = 0.2 mm.

The floor of the neural canal consists of an intensely remodelled lamellar osseous tissue displaying numerous cementing lines of resorption and Howship's lacunae. This structure is probably the result of a complex resorption/reconstruction process related to both the increase in diameter of the neural canal during growth, and the remodelling of the inner side of the periosteal deposits in the dorsal territory of the centrum. Local remodelling can be so intense that parts of the floor of the neural canal are entirely destroyed, the inner cavities of the centrum thus communicating with the neural canal.

In species for which several specimens of different size were available (*Eunectes murinus*, *Broghammerus reticulatus*, *Tupinambis teguixin*, *V. exanthematicus*), compactness indices are similarly independent of the size of the specimens (cf. Table 1). Moreover, the relative area of primary PBCL does not vary according to size (cf. Table 1). Remodelling seems therefore to start at an early stage of development and appears to remain roughly constant throughout growth.

The section from the specimen of *V. exanthematicus* injected with fluorochromes shows that the growth in length of the centrum is much more active posteriorly than anteriorly. In most classical sections, the margin between primary periosteal deposits and remodelled endosteo-enchondral tissues is clearly visible in the ventral part of the centrum, thus revealing the contours of the originally triangular formations (cones in 3D) of endosteo-enchondral bone resulting from the growth in length of the centrum (Fig. 3A). Therefore, despite the presence of wide lacunae in the deep centrum, the position of the neutral point, marking the origin of the growth in length and diameter of the centrum, could be approximated in 54 taxa (23 lizards and 31 snakes).

Transverse sections

In transverse sections, there is no discontinuity of the osseous tissues between the centrum, neural arch and neural spine, regardless of the species and the size of the specimen. In most taxa, resorption leads to the formation of wide cavities susceptible to fuse with each other, thus creating very large hollow spaces separated only by thin trabeculae. This confers a peculiar architecture to the vertebrae; in cross-section, they appear to be made of two more or less concentric osseous rings (tubular structures in volume) connected by some thin radial trabeculae

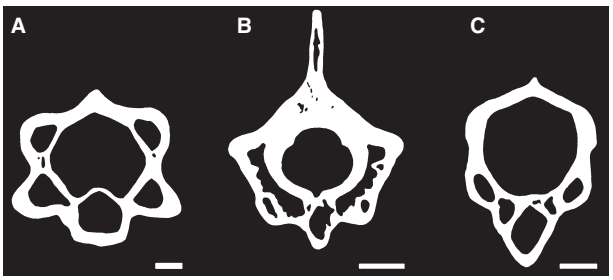

Fig. 5 Schematic drawing illustrating the various patterns observed in transverse sections. White, bone; black, cavities. (A) *Agama atra* MNHN AC 1887 881; note the typical structure in 'double rings separated by only few trabeculae' in the entire vertebra except the neural spine. Scale bar = 500 μm. (B) *Eunectes murinus* MNHN SQ-Vert 9; note the absence of cavities in the neural arch. Scale bar = 5 mm; (C) *Calumma nasutum* MNHN 6643F; note the restriction of cavities to the centrum. Scale bar = 200 μm.

(Fig. 3B). The peripheral tube (ring on section) corresponds to the cortex of the vertebra and is made of a parallel-fibered tissue housing radial simple vascular canals in large-sized taxa (cf. observations in longitudinal sections); the inner ring, made of highly remodelled true lamellar bone (as demonstrated by the numerous cementing lines of resorption and Howships's lacunae), corresponds to the wall of the neural canal. However, in several taxa (e.g. *Dipsosaurus*, *Eunectes*, *Morelia*), the neural arch lacks cavities (Fig. 5B) and in some others (e.g. *Brookesia*, *Calumma, Dendroaspis*, *Xenopeltis*), both the neural arch and neural spine are compact such that the structure of the double ring is restricted to the centrum (Fig. 5C). Moreover, in *Cylindrophis ruffus*, there is a peculiar inhibition of periosteal bone resorption that confers a strong compactness to the transverse section.

Quantitative analysis

In longitudinal sections, the vertebral centra of the squamates examined in our study display global compactness indices (CIs) ranging from 38.5% in *Varanus griseus* to 88.8% in *Hydrophis* sp. (Table 1; mean value = 64.9%). The relative area occupied by primary periosteal deposits (PBCL) varies between taxa and specimens (from 8.7% in *Amblyrhynchus cristatus* to 55.2% in *Bitis arietans*), with a mean value of 25.8%. Vertebral compactness as estimated on transverse sections ranges from 40.3% in *T. teguixin* to 96.1% in *C. ruffus* (Table 1; mean value = 68.0%).

A correlation between CL and the number of cavities in longitudinal section (TNCL) reveals a strong correlation ($r = 0.87$; $P < 0.001$; Fig. 6A). Moreover, this correlation remained significant after taking into account the evolutionary relationships between species (analysis on independent contrasts: $r = 0.73$; $P < 0.001$), suggesting that these patterns are independent of phylogenetic relatedness. The correlation between CL and TNCT was also significant but explained less of the variation in the data set in both traditional ($r = 0.59$; $P < 0.001$; Fig. 6B) and independent contrast analyses ($r = 0.39$; $P = 0.017$). This general correlation between vertebral size and the number of cavities thus appears to be a general trend throughout the evolution of squamate vertebrae with the evolution of larger vertebrae being associated with the evolution of more cavities. Whereas transverse sections only expose bone of periosteal origin, longitudinal sections expose bone of both endosteo-enchondral and periosteal origin. This trend appears thus to result from an increase of the number of cavities with specimen size in the endosteo-enchondral rather than in the periosteal territory. A correlation analysis between CIs and TNCL reveals no correlation in both traditional ($r = 0.14$; $P = 0.26$; Fig. 7A) and independent contrast analyses ($r = 0.098$; $P = 0.57$). However, the correlation between CTs and TNCT indicated a significant albeit weak correlation in traditional analysis ($r = -0.35$; $P = 0.004$; Fig. 7B), which did not remain after taking into account the evolutionary relationships between species ($r = 0.22$; $P = 0.20$). Thus, the evolution of more compact vertebrae is not associated with a change in the number of cavities observed in the vertebrae.

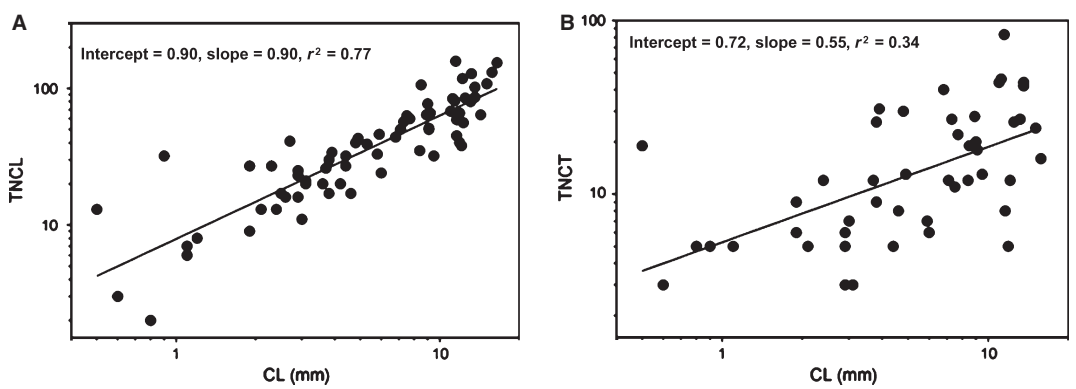

Fig. 6 Graphs illustrating the correlations between centrum length (CL) and the total number of cavities in (A) longitudinal (TNCL) and (B) transverse (TNCT) sections.

The correlation between Cls and PBCL ($P < 0.001$; $r = 0.71$), on the one hand, and Cts and PBCT ($P < 0.001$; $r = 0.89$), on the other hand (Fig. 8), was also significant.

Analyses of (co)variance testing for differences in vertebral compactness between animals utilising different habitats detected no differences in the number of cavities in longitudinal (ANCOVA; $F_{4,31} = 1.5$; $P = 0.23$) or transverse (ANCOVA; $F_{4,31} = 1.75$; $P = 0.17$) sections. Bone compactness in longitudinal section was also comparable between groups (ANOVA; $F_{4,32} = 1.2$; $P = 0.33$). The degree of Cts was, however, significantly different between animals occupying different habitats (ANOVA; $F_{4,32} = 2.79$; $P = 0.043$) with fossorial species having the most compact and terrestrial species having the least compact vertebrae. Other habitat groups (climbers, generalists) were intermediate between aquatic and terrestrial species. When taking into account the relationships among species, the difference between groups was no longer significant ($F_{trad} = 2.79 < F_{phyl} = 4.06$; $p_{phyl} = 0.17$), indicating a significant phylogenetic signal in the data. Indeed, inspection of Fig. 2 suggests an unequal distribution of taxa among lizards and snakes which, given the known differences between these two groups, may reduce our statistical power to detect an adaptive signal.

The relative compactness as estimated on longitudinal sections (Cls) differs significantly between snakes and lizards ($F_{1,35} = 14.45$; $P = 0.001$), being higher in snakes (70.7%) than in lizards (59.2%). Similarly, relative compactness as estimated on transverse sections (Cts) also differs significantly between snakes and lizards ($F_{1,35} = 15.29$; $P < 0.001$), being higher in the former (75.7%) than in the latter (61.2%). Mean PBCL (*t*-test; $t = 6.86$; $P < 0.001$) and mean PBCT (*t*-test; $t = 4.93$; $P < 0.001$) are also significantly different between lizards and snakes (PBCL: 32.5% in snakes vs. 17.1% in lizards; PBCT: 60.5% in snakes vs. 40.7% in lizards). The NPPi was, however, not different (*t*-test; $t = 0.610$; $P = 0.55$) between snakes (73.5%) and lizards (74.8%), suggesting that the respective contributions of cotylar and condylar epiphyses to growth are similar in lizards and snakes. The CPi was significantly different in lizards and snakes ($U = 96$; $P < 0{,}001$), being higher in the former (45.2%) than in the latter (28.0%), thus suggesting that vertebral growth in diameter relative to growth in length is more important in snakes.

Discussion

Vertebral growth pattern

The observations presented here suggest the following growth pattern for squamate vertebral centra: growth in length of the centra relies on a process of endochondral ossification (cf. Francillon-Vieillot et al. 1990). Conversely, growth in diameter results from centrifugal deposits of parallel-fibered, primary periosteal tissue. Initially very compact, this tissue undergoes extensive remodelling in its deepest part. This remodelling process is characterised in squamates by an imbalance between bone resorption and reconstruction; osteoclast activity is only partially balanced by that of the osteoblasts. Consequently, the amount of eroded bone is not entirely replaced by secondary reconstructive tissue. Because of this reconstruction deficit, which increases toward the core of the centrum, the originally compact periosteal cortex becomes cancellous and turns into a loose, intensely remodelled spongiosa in the core of the centrum. As a result, the inner architecture of squamate vertebral centra resembles that of a tubular bone.

Our observations show that this remodelling imbalance already occurs in juvenile specimens. Because compactness indices remain relatively constant during growth, it seems that some equilibrium between this remodelling imbalance and growth is reached early during development and remains constant throughout life. Our data strongly suggest that the size of cavities and their number vary with bone size, but not with bone compactness.

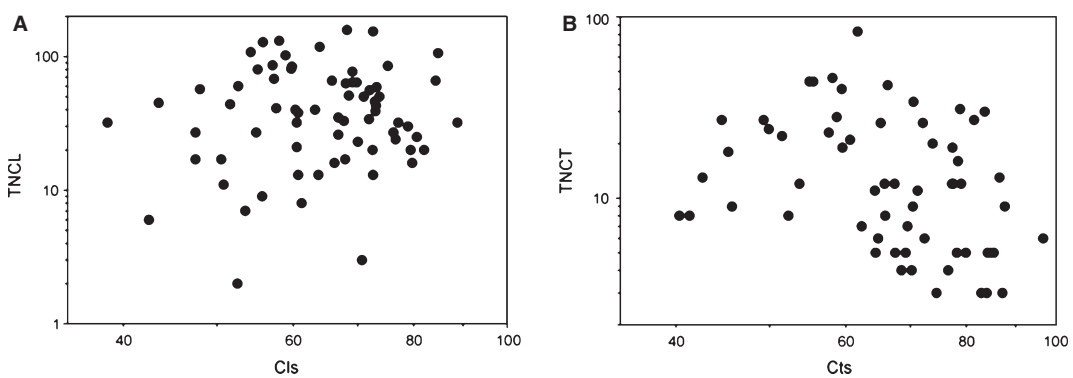

Fig. 7 Graphs illustrating the correlations between (A) global compactness (Cls) and the total number of cavities in longitudinal sections (TNCL), and (B) global compactness (Cts) and the total number of cavities in transverse sections (TNCT).

Centrum growth asymmetry

In longitudinal sections, the unequal distances of the cotyle and condyle from the neutral point reveal that growth in length is asymmetrical in squamate vertebrae, being much faster in the caudal (representing three-quarters of the total growth in length) than in the cranial direction. Moreover, most of the growth in diameter of the centrum occurs in the ventral region, the development of the neural canal interfering with dorsal growth.

Differences within squamates

Growth in diameter relative to growth in length is proportionally more important in snakes than in lizards, as illustrated by the differences in the CPi between the two groups. It remains currently unclear whether this is caused by an increase in growth speed or growth duration. As periosteal bone is pseudolamellar in both lizards and snakes, and similarly vascularised (i.e. only in the largest taxa), it does not seem that periosteal growth speed is faster in snakes than in lizards. This observation, combined with the correlations between Cls and PBCL, on the one hand, and Cts and PBCT, on the other hand, suggests that the higher compactness observed in snakes may result from both a less intense resorption of primary periosteal bone, and more abundant periosteal deposits. These differences between lizards and snakes could suggest that limbless forms need relatively more robust vertebrae than limbed forms. However, whereas this hypothesis is supported by the high Cls and notably Cts values observed in the limbless species *Amphisbaena alba*, it is not supported by the values obtained for *Anguis fragilis* (whose Cls value notably does not even reach the mean lizard Cls value).

Ecological correlates

Our preliminary analyses testing for associations between vertebral density and mode of life in squamates gave mixed results. Whereas our traditional analyses suggest that there are indeed differences in the degree of compactness of the vertebrae between squamates occupying different habitats, these were not borne out by our phylogenetically informed analyses suggesting the presence of distinct phylogenetic signal in our data set. However, the direction of the differences detected in the traditional analysis was congruent with the *a-priori* predictions that fossorial species have denser vertebrae than terrestrial species. Aquatic species had vertebrae of intermediate density, again as predicted. Generalists and climbers were not clearly differentiated from terrestrial ground-dwelling species, suggesting that there may not be any constraints associated with this life-style, at least with respect to the degree of vertebral compactness. The lack of significance in our phylogentically informed analyses is probably due, at least partially, to a clustering of ecological groups with clades (see Vanhooydonck & Van Damme, 1999). As most of the fossorial and aquatic taxa in our analysis were snakes, and as snakes appear to have denser vertebrae than other squamates, this may have introduced a bias in our analysis.

Comparison with non-squamate taxa

Longitudinal and transverse sections from the comparative material reveal a striking difference in vertebral inner architecture between squamate and non-squamate taxa. Indeed, in the longitudinal sections of most non-squamate taxa, most of the centrum is occupied by a relatively uniform spongiosa whose trabeculae are predominantly oriented in a sagittal direction (Fig. 9A). Compact periosteal bone is limited, as in squamates, to narrow cortices along the ventral and, to a lesser extent, the dorsal borders of the centrum (Fig. 9A). The inner architecture of the crocodile centrum differs from this general trend, and shares features with the centrum of squamates. Whereas the endosteoenchondral spongiosa in this species consists of a tight network of trabeculae enclosing cavities predominantly oriented in a sagittal direction (which differs from the condition observed in squamates), the spongiosa of periosteal

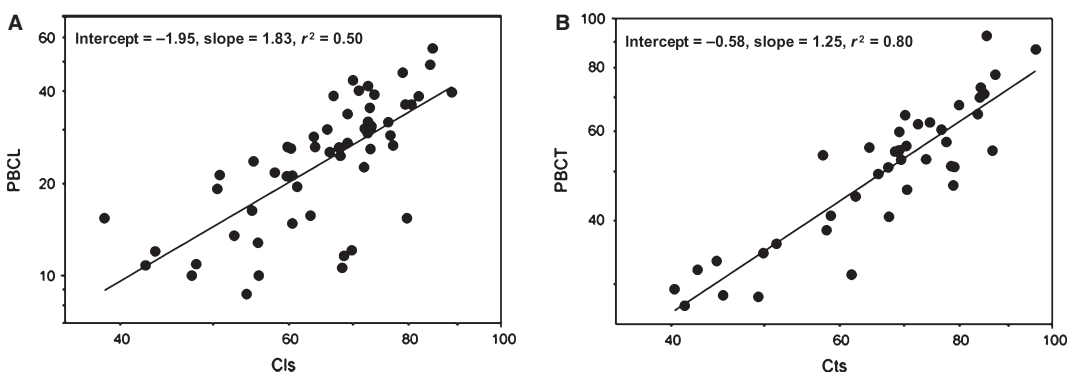

Fig. 8 Graphs illustrating the correlations between (A) global compactness (Cls) and the relative area of primary periosteal bone in longitudinal sections (PBCL), and (B) global compactness (Cts) and the relative area of primary periosteal bone in transverse sections (PBCT).

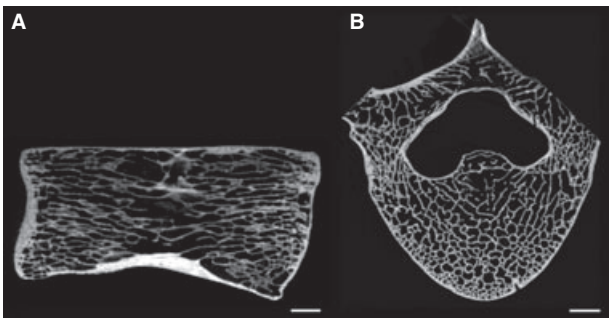

Fig. 9 (A) *Capreolus capreolus*. MNHN AC (no ref.). Virtual longitudinal section of the vertebral centrum. (B) *Otaria byronia*. MNHN AC 1884-862. Virtual partial transverse section of the vertebra. Scale bars = 5 mm.

origin is loose with relatively large, randomly shaped intertrabecular spaces.

In transverse sections, most non-squamate vertebrae are almost entirely cancellous. They display two osseous walls surrounding, respectively, the neural canal and outer border of the bone, whose thickness varies according to taxa (Fig. 9B). These walls are connected by a tight and relatively uniform trabecular network (Fig. 9B). Consistent with what is observed in longitudinal sections, the trabecular network in *Crocodylus niloticus* is much less tight and uniform than in the other non-squamate tetrapods. To a lesser extent, this is also the case for *Meles* and *Oryctolagus*, whose spongiosae are less tight in longitudinal section than those of other non-squamate tetrapods. However, regardless of the variation observed among non-squamate tetrapods, they all display a microanatomical organisation distinctly different from that observed in squamates.

Concluding remarks

Squamate vertebral inner structure differs from that of other tetrapods. This peculiar structure, which characteristically evokes that of a tubular bone, results from an imbalance between resorption and redeposition during bone remodelling. It is a typical trait of squamate vertebral osteogenesis that may bear a functional significance. Although our data suggest adaptive patterns in the vertebral microstructure, much work remains to be done in order to better understand squamate vertebral microanatomy. Further studies based on a much broader sample illustrating various modes of life (e.g. limbless lizards from various families; various aquatic taxa) are needed to better understand the relationships between ecology and mode of life, the musculo-skeletal system, and the vertebral internal architecture in squamates. The use of high-resolution phase contrast X-ray synchrotron microtomography for virtual histology (e.g. Tafforeau & Smith, 2008) could reveal itself useful in biomechanical studies as it allows the investigation of the 3D distribution of the different osseous tissues in a non-destructive manner.

Acknowledgements

We warmly thank I. Ineich (Muséum National d'Histoire Naturelle, Paris, France), W. Böhme (Museum Alexander Koenig, Bonn, Germany), J. Castanet (Université Pierre et Marie Curie, Paris, France) and La Ferme Tropicale (Paris, France) for the loan or donation of specimens, and M. Dumont (Max Planck Institut für Eisenforschung, Düsseldorf, Germany) and A. Mirales (MNHN, Paris, France) for allowing the use of their scans of the specimens of *Tribolonotus*, and *Enhydra*, *Otaria* and *Capreolus*, respectively. Particular thanks to H. Lamrous (Université Pierre et Marie Curie, Paris, France) for her help in the realisation of the sections. Thanks to Roberto Macchiarelli (Université de Poitiers and MNHN, Paris, France) and Paul Sardini (Université de Poitiers, France) for access to the Centre de Microtomographie of the Université de Poitiers, to the ESRF (Grenoble, France) for providing beamtime and support, and to N. Pollet (CNRS/Genopole, Evry, France) and E. Boller (ESRF, Grenoble, France) for their help during experiments. We also thank the ANR (LOCOMO) 06-BLAN-0132-02 for financial support. We are also grateful to M. Geze and J. Jovet for providing and accommodating the use of Amira software at CEMIM (MNHN, Paris, France), and to S. Couette and A. Boura (MNHN, Paris, France) for their help with statistics.

Authors' contribution

Acquisition of data: Alexandra Houssaye, Arnaud Mazurier, Paul Tafforeau, Renaud Boistel and Vivian de Buffrénil; data analysis: Alexandra Houssaye; help in method of data analysis: Renaud Boistel, Anthony Herrel and Virginie Volpato; drafting of the manuscript: Alexandra Houssaye; critical revision of the manuscript: all authors.

References

Abramoff MD, Magelhaes PJ, Ram SJ (2004) Image processing with ImageJ. *Biophoton Int* **11**, 36–42.

Ast JC (2001) Mitochondrial DNA evidence and evolution in Varanoidea (Squamata). *Cladistics* **17**, 211–226.

de Buffrénil V, Rage J-C (1993) La ''pachyostose'' vertébrale de *Simoliophis* (Reptilia, Squamata): données comparatives et considérations fonctionnelles. *Ann Paléontol* **79**, 315–335.

de Buffrénil V, Sire J-Y, Schoevaert D (1986) Comparaison de la structure et du volume squelettiques entre un delphinidé (*Delphinus delphis* L.) et un mammifère terrestre (*Panthera leo* L.). *Can J Zool* **64**, 1750–1756.

de Buffrénil V, Bardet N, Pereda Suberbiola X, et al. (2008) Specialization of bone structure in *Pachyvaranus crassispondylus* Arambourg, 1952, an aquatic squamate from the Late Cretaceous of the southern Tethyan margin. *Lethaia* **41**, 59–69.

Castanet J (1982) Recherches sur la croissance du tissu osseux des reptiles. Application: la méthode squelettochronologique. PhD thesis. Paris: Université Paris VII.

Castoe TA, Parkinson CL (2006) Bayesian mixed models and the phylogeny of pitvipers (Viperidae: Serpentes). *Mol Phylogenet Evol* **39**, 91–110.

Diaz-Uriarte R, Garland T Jr (1998) Effects of branch lengths errors on the performance of phylogenetically independent contrasts. *Syst Biol* **47**, 654–672.

Francillon-Vieillot H, de Buffrénil V, Castanet J, et al. (1990) Microstructure and mineralization of vertebrate skeletal tissues. In *Skeletal Biomineralization: Patterns, Processes and Evolutionary Trends*. (ed. Carter JG), pp. 471–529. New York: Van Nostrand Reinhold.

Garland T Jr, Harvey PH, Ives AR (1992) Procedures for the analysis of comparative data using phylogenetically independent contrasts. *Syst Biol* **41**, 18–32.

Garland T Jr, Dickerman AW, Janis CM, et al. (1993) Phylogenetic analysis of covariance by computer simulation. *Syst Biol* **42**, 265–292.

Garland T Jr, Midford PE, Ives AR (1999) An introduction to phylogenetically based statistical methods, with a new method for confidence intervals on ancestral states. *Am Zool* **39**, 374–388.

Gasc J-P (1976) Snake vertebrae – a mechanism or merely a taxonomist's toy? In *Morphology and Biology of Reptiles: Linnean Society Symposium Series*. (eds Bellairs ADA, Cox CB), pp. 177–190. New York: Academic Press.

Gasc J-P (1977) Morphologie vertébrale et mode de locomotion chez les squamates: supériorité de l'analyse morpho-fonctionnelle sur la morphologie descriptive. *Bull Biol Fr Belg* **111**, 29–44.

Heggeness MH, Doherty BJ (1997) The trabecular anatomy of thoracolumbar vertebrae: implications for burst fractures. *J Anat* **191**, 309–312.

Hengsberger S, Ammann P, Legros B, et al. (2005) Intrinsic bone tissue properties in adult rat vertebrae: modulation by dietary protein. *Bone* **36**, 134–141.

Hoffstetter R, Gasc J-P (1969) Vertebrae and ribs of modern reptiles. In *Biology of the Reptilia. Vol. 1, Morphology A*. (ed. Gans C), pp. 201–310. London and New York: Academic Press.

Houssaye A, de Buffrénil V, Rage J-C, et al. (2008) An analysis of vertebral 'pachyostosis' in *Carentonosaurus mineaui* (Mosasauroidea, Squamata) from the Cenomanian (early Late Cretaceous) of France, with comments on its phylogenetic and functional significance. *J Vertebr Paleontol* **28**, 685–691.

Kelly CMR, Barkera NP, Villet MH, et al. (2009) Phylogeny, biogeography and classification of the snake superfamily Elapoidea: a rapid radiation in the late Eocene. *Cladistics* **25**, 38–63.

Lee MSY (2009) Hidden support from unpromising data sets strongly unites snakes with anguimorph 'lizards'. *J Evol Biol* **22**, 1308–1316.

Lee MSY, Hugall AF, Lawson R, et al. (2007) Phylogeny of snakes (Serpentes): combining morphological and molecular data in likelihood, Bayesian and parsimony analyses. *System Biodiver* **5**, 371–389.

Martins EP, Garland T Jr (1991) Phylogenetic analyses of the correlated evolution of continuous characters: a simulation study. *Evolution* **45**, 534–557.

Mazurier A, Volpato V, Macchiarelli R (2006) Improved non-invasive microstructural analysis of fossil tissues by means of SR-microtomography. *Appl Phys A* **83**, 229–233.

Moon BR (1999) Testing an inference of function from structure: snake vertebrae do the twist. *J Morphol* **241**, 217–225.

O'Reilly JC, Ritter DA, Carrier DR (1997) Hydrostatic locomotion in a limbless tetrapod. *Nature* **386**, 269–272.

Ritter D (1996) Axial muscle function during lizard locomotion. *J Exp Biol* **199**, 2499–2510.

Tafforeau P, Smith TM (2008) Nondestructive imaging of hominoid dental microstructure using phase contrast X-ray synchrotron microtomography. *J Hum Evol* **54**, 272–278.

Tafforeau P, Boistel R, Boller E, et al. (2006) Applications of X-ray synchrotron microtomography for non-destructive 3D studies of paleontological specimens. *Appl Phys A* **83**, 195–202.

Vanhooydonck B, Van Damme R (1999) Evolutionary relationships between body shape and habitat use in lacertid lizards. *Evol Ecol Res* **1**, 785–805.

Wiens JJ, Hollingsworth BD (2000) War of the Iguanas: conflicting molecular and morphological phylogenies and long-branch attraction in iguanid lizards. *Syst Biol* **49**, 143–159.